16th World Conference on Earthquake, 16WCEE 2017

Santiago Chile, January 9th to 13th 2017

Paper N° 121 (Abstract ID)

Registration Code: S-T1456201148

DAMAGE OCCURRENCE MECHANISM OF PLAIN CONCRETE PIERS FOR RAILROAD BRIDGES DURING EARTHQUKAES AND SEISMIC MEASURES

A. Furukawa [(1)], A. Mizukami [(2)], J. Kiyono [(3)]

[(1)] *Associate Professor, Dept. of Urban Management, Kyoto University, furukawa,aiko.3w@kyoto-u.ac.jp*
[(2)] *Engineer, Japan Railway Construction, Transport and Technology Agency (JRTT), mizukamiakira1029@gmail.com*
[(3)] *Professor, Dept. of Urban Management, Kyoto University, kiyono.junji.5x@kyoto-u.ac.jp*

Abstract

In the past earthquakes such as the 2004 Niigata-ken Chuetsu Earthquake and the 2011 off the Pacific coast of Tohoku Earthquake in Japan, serious damage to plain concrete piers of railroad bridges has been caused. The typical damage is horizontal gap at the cold joint of the pier and falling down of concrete pieces from the pier under the cold joint. It is necessary to understand the damage occurrence mechanism and to develop effective seismic measures to prevent serious damage in the future earthquakes. With this background, this study analyzed the seismic behavior of a plain concrete pier using the refined distinct element method (Refined DEM). The analyzed model is a plain concrete pier of Uonogawa bridge which is located in Niigata Prefecture and damaged during the 2004 Niigata-ken Chuetsu Earthquake. The damage occurrence mechanism was investigated through the analysis. As for the seismic measures, the RC jacketing method is generally used, but this method cannot be used for piers in the river since the cross-sectional area of the river is reduced. For this purpose, the seismic measures which does not reduce the cross-sectional area of the river is required. Therefore, this study considers the seismic measures which does not affect the cross-sectional area of the river, and verify the validity of the measures through the analysis.

Keywords: plain concrete pier; damage occurrence mechanism; seismic measure; earthquake; Refined DEM

1. Introduction

In the past earthquakes, serious damage to plain concrete piers of railroad bridges has been caused [1, 2, 3, 4]. The typical damage is horizontal gap at the cold joint of a pier and falling down of concrete pieces from the pier under the cold joint. It is necessary to understand the damage occurrence mechanism and to develop effective seismic measures to prevent serious damage in the future earthquakes. With this background, this study analyzed the seismic behavior of a plain concrete pier using the refined DEM [5], investigated the damage occurrence mechanism, and verified the validity of two seismic measures. It was found that the friction and collision forces from the upper pier above the cold joint caused the tensile failure of the pier under the cold joint. The effectiveness of two seismic measures was found to be limited since the concrete contacting the reinforcement material suffered from damage.

2. Analysis Method

2.1 Refined DEM

This study employs a refined DEM [5] to simulate a series of structural dynamic behaviors from elastic to failure to collapse phenomena. A structure is modeled as an assembly of rigid elements, and interaction between elements is modeled with multiple springs and multiple dashpots that are attached to the surfaces of elements. Fig. 2 (a) shows a spring for computing the restoring force (restoring spring), which models the elasticity of elements. The restoring spring is set between continuous elements. Fig. 2 (b) shows a spring and dashpot for computing the contact force (contact spring and dashpot) and modeling the contact, separation and recontact between elements. The dashpots are introduced to express energy dissipation due to the contact. Structural failure is modeled as breakage of the restoring spring (Fig. 2 (c)), at which time the restoring spring is replaced with a contact spring and a contact dashpot (Fig. 2 (b)). Structural collapse behavior is obtained using these springs and dashpots. The elements shown in Figs. 2 (a) and (b) are rectangular parallelepipeds, but the method does not limit the geometry of the elements. The surface of an element is divided into small segments as shown in Fig. 2 (d). A segment in the figure is rectangular, but the method does not limit the geometry of the segment. The black points indicate the representative point of each segment, and the relative displacement or contact displacement between elements is computed for these points. Such points are referred to as contact points or master points in this study. One restoring spring and one combination of contact spring and dashpot are attached to one segment (Fig. 2 (e)) at each of the representative points in Fig. 2 (d). The spring constant for each segment is derived on the basis of the stress–strain relationship of the material and the segment area. Forces acting on each element are obtained by summing the restoring force, contact force and other external forces such as the gravitational force and inertial force of an earthquake. The behavior of an element consists of the translational behavior of the center of gravity and the rotational behavior around the center of gravity. The translational and rotational behaviors of each element are computed explicitly by solving Newton's law of motion and Euler's equation of motion.

Fig. 1 – Uonogawa Bridge damaged during the 2014 Niigata-ken Chuetsu Earthquake [3]

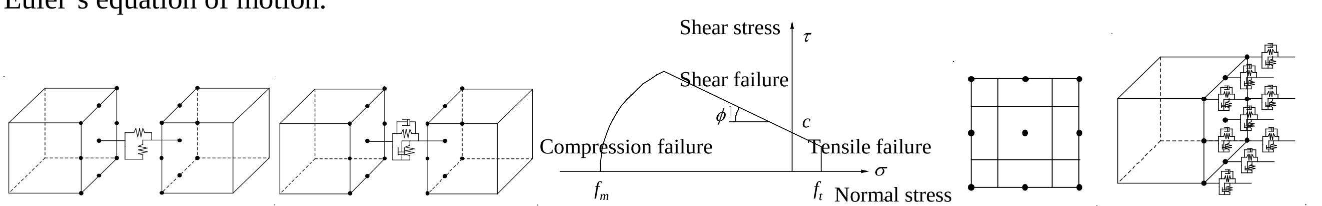

(a) Restoring spring (b) Contact spring and dashpot (c) Failure judgment (d) Segments and contact points (e) Multiple springs & dashpots

Fig. 2 – Basic concept of analysis method

2.2 Spring constant of each element

There are two types of springs, namely restoring and contact springs. It is considered that each segment has its own spring. The springs are set for both the normal and shear directions of the surface. The spring constants per area in the normal and shear directions, k_n and k_s, are obtained as follows.

$$k_n = \frac{E}{(1-\nu^2)\ell}, \quad k_s = \frac{E}{2(1+\nu)\ell} \tag{1}$$

where E is Young's modulus, ν is Poisson's ratio, and ℓ is the distance from the surface at which the spring is connected to the center of gravity.

2.3 Modeling of elastic behavior

It is assumed that two elements, A and B, are continuous, and that a contact point of element A is continuous with element B. Let G_A and G_B be the centers of gravity of elements A and B respectively. Let ℓ_A be the distance from G_A to the surface of element A in contact. Let ℓ_B be the distance from G_B to the surface of element B in contact. Let E_A and E_B be Young's moduli and ν_A and ν_B be Poisson's ratios of elements A and B.
The spring constants per area for the elements A and B are obtained from Eq. (1). Assuming that these springs are connected in series, the spring constants between elements per area, $\bar{k}_n$ and $\bar{k}_s$, are

$$\bar{k}_n = \frac{1}{\dfrac{\ell_A}{E_A/(1-\nu_A^2)} + \dfrac{\ell_B}{E_B/(1-\nu_B^2)}}, \quad \bar{k}_s = \frac{1}{\dfrac{\ell_A}{E_A/2(1+\nu_A)} + \dfrac{\ell_B}{E_B/2(1+\nu_B)}} \tag{2}$$

The spring constant between elements connected by mortar is also obtained in a similar manner. For example, in masonry structures, bricks are often connected with mortar. In such cases, the spring constant per area between elements (bricks) is obtained as

$$\bar{k}_n = \frac{1}{\dfrac{\ell_A - t_M/2}{E_A/(1-\nu_A^2)} + \dfrac{t_M}{E_M/(1-\nu_M^2)} + \dfrac{\ell_B - t_M/2}{E_B/(1-\nu_B^2)}}, \quad \bar{k}_s = \frac{1}{\dfrac{\ell_A - t_M/2}{E_A/2(1+\nu_A)} + \dfrac{t_M}{E_M/2(1+\nu_M)} + \dfrac{\ell_B - t_M/2}{E_B/2(1+\nu_B)}} \tag{3}$$

where t_M is the mortar thickness and E_M is Young's modulus and ν_M is Poisson's ratio of the mortar. The normal direction of forces is the direction perpendicular to the surface of the master point of element A.
Let σ and τ be the normal and shear stresses acting at the contact point, and u_n and u_s be the relative displacements between the adjacent master and slave points in the normal and shear directions. The relation between traction (σ, τ) and relative displacements (u_n, u_s) is then written as

$$\sigma = \bar{k}_n u_n, \quad \tau = \bar{k}_s u_s. \tag{4}$$

The method cannot handle the poisson's effect since it considers the contact between two elements.

2.4 Modeling of failure phenomena

The elastic behavior of structures is demonstrated by the multiple restoring springs between continuous elements until the restoring force of a spring reaches its elastic limit. The elastic limits are modeled using criteria of tension, shear and compression failure. When a spring reaches one of these limits, it is judged that failure has occurred at the segment of the spring. After the failure, the restoring spring is replaced with a contact spring and dashpot at this segment. The method can trace the expansion of failure between elements. The three failure modes—namely, tension, shear and compression failure modes—are defined as follows.

2.4.1 Tension failure mode

In the tension failure mode, the parameter considered is the tensile strength f_t. When the normal stress of a spring σ exceeds the tensile strength, the restoring spring is assumed to be broken by the tension failure. The yield function has the following form (Fig. 2(c)).

$$f_1(\sigma) = \sigma - f_t \tag{5}$$

The normal restoring stress cannot exceed this limit.

2.4.2 Shear failure mode

For the shear failure mode, the Coulomb friction envelope is used. The parameters considered are the bond strength c and friction angle ϕ. The yield function has the following form (Fig. 2(c)).

$$f_2(\sigma) = |\tau| + \sigma\tan\phi - c \tag{6}$$

The shear restoring stress cannot exceed this limit.

2.4.3 Compression failure mode

For the compression mode, an ellipsoid cap model is used. The yield function has the form (Fig. 2(c)) as.

$$f_3(\sigma) = \sigma^2 + C_s\tau^2 - f_m{}^2 \tag{7}$$

where f_m is the compressive strength and Cs is the material model parameter. $Cs = 9$ is adopted on the basis of past research [6]. When the restoring stress exceeds this limit, both the normal and shear restoring stresses are reduced in the same proportion to meet this limit.

2.5 Modeling of contact and recontact between elements

If a segment of an element is in contact with another element with which the segment is not continuous via the restoring spring, the contact spring and dashpot generate the contact force. Contact between a segment and the surface of another element is detected at each time step for all segments that are not continuous with other elements via a restoring spring. The spring constant and the contact forces in the normal and shear directions are calculated in the same manner as for the restoring force. The differences from the case for the restoring force are that the contact force is generated only while the compression force acts and that the shear force is bounded by the friction limit.

$$\tau = \sigma\tan\phi \tag{8}$$

where ϕ is the friction angle. The dashpot is introduced to express the energy dissipation of the contact. The damping coefficient per area is calculated as follows.

$$c_n = 2h_n\sqrt{m_{ave}k_n}\,,\ \ c_s = 2h_s\sqrt{m_{ave}k_s} \tag{9}$$

where h_n and h_s are the damping constants for the normal and shear directions. m_{ave} is the equivalent mass per area relevant to this contact. In this study, m_{ave} is calculated as

$$m_{ave} = \rho_A\ell_A + \rho_B\ell_B \tag{10}$$

where ρ_A and ρ_B are the mass densities of elements A and B. The damping constants should be evaluated according to the properties of the elements, but this study adopts critical damping ($h_n = h_s = 1.0$) by considering that most structural components tend not to bounce greatly and their oscillation tends to disappear quickly when they collide with each other.

2.6 Equations of Motion

The equations of motion can be constructed using the restoring and contact forces and other external forces. The motion of each element is obtained by solving the two equations of motion. One is the equation for the translational motion of the center of gravity, and the other is the equation for the rotational motion around the center of gravity. By solving the equations of motion step by step, the position of each element can be traced, and the whole structural behavior can be obtained.

3. Analysis of Seismic Behavior of 14 Pier of Uonogawa Bridge

3.1 Target structure

In this study, pier 14 of Uonogawa bridge was studied, which suffered dislocation at the cold joint in the transverse direction during the 2004 Niigata-ken Chuetsu Earthquake (Fig.2). The overview and section of the pier is shown in Fig. 3. The higher, the section area becomes smaller, and the cold joint is at the height of 6.619 from the bottom of the footing.

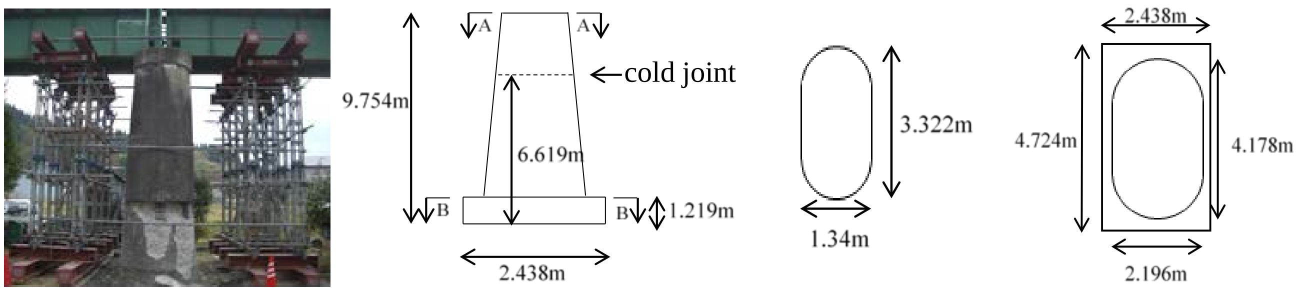

(a) Photo [4] (b)Overview (c) Sectional view(A-A') (d) Sectional view (B-B')

Fig.3 – Photo and dimension of pier 14 of Uonogawa bridge (Left:north-east, right: south-west)

3.2 Analytical model

Fig.4 illustrates the analytical model ot pier 14 of Uonogawa bridge without reinforcement. The *x*, *y*, *z* indicates the north-east, north-west, and upward directions, respectively. The pier is modeled by reducing the section area every 0.2m in *z* direction.

The material properties of concrete used in the analysis is shown in Table 1. These valueswere determined based on the double shear test and compression test done by West Japan Railway Company [7]. The cylinder-shaped specimen who has the radius of 150mm and the length of 100mm were taken from the existing plain concrete piers of Kisei Main Line in Wakayama Prefecture. The specimen were not taken from pier 14 of Uonogawa bridge, but the values of Wwakayama were used since their construction period was almost the same. As for the shear strength of the cold joint, the cohesion and friction angle were obtained from the double shear tests. The specimen was take from the cold joint part, and its half was taken from the upper part and the other half was taken from the lower part than the cold joint. The cold joint was not smoth, and it seemed that the shar strength of the cold joint were depending on the smoothness of the joint. The tensile strength of the cold joint was assumed to be 0 since the specimen separated easily at the joint with the small impact. As for the compression strength of the cold joint, the same value with the compression strength of the concrete was used. It is noted that no compression failure occured at the cold joint, therefore the compression strength used for the cold joint does not affect the analytical results.

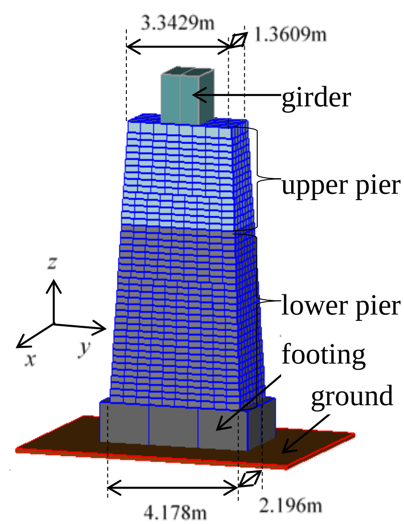

Fig.4 – Analytical model without reinforcement

Table 1–Material properties of concrete

(a) Material properties

Densigy (kg/m^3)	2.3×10^3
Young's module (N/m^2)	2.2×10^{10}
Poisson's ratio	0.20

(b)Strength between elements

	Concrete	Cold joint
Tensile strength f_t (N/m^2)	1.75×10^6	0
Cohesion c (N/m^2)	5.8×10^5	1.62×10^4
Friction angle ϕ (rad)	0	0.52
Compression strength f_m (N/m^2)	2.39×10^7	2.39×10^7

The compression strength of the concrete was obtained from six core samples, three from the upper part and three from the lower part than the cold joint. The tensile and shear strength of the concrete was calculated from the compression strength based on the equations shown in the specification of railway structures [8]. The compression strength of the upper part valies 24.6-39.4N/mm^2 and that of the lower part valies 23.9-33.5N/mm^2. Since the difference of the compression strength is small between the upper and the lower parts, the constant compression strength, the minimum compression strength 23.9N/mm^2 was adopted for the both upper and lower parts.

In the real structure, the pier supports the weight from the steel girder. The weight of the girder was modeled by the rectangular-parallellepiped element whose weight is 124.8kN. The material is steel, the density is 5.28×10^3kg/m^3, Young's module is 2.0×10^{11}N/m^2, and the Poisson's ratio is 0.30. To apply the same inertial force due to the earthquake, the height of the girder element was adjusted. Since the bearing support was not broken during the 2004 Niigata-ken Chuetsu Earthquake, the large values were used for the tensile, shear and compression strength between the girder and the top of the pier so that the two parts are not separated at the interface. The footing was modeled by the assemble of 1.22m×1.57m× 1.2m elements, and the girder was modeled by the assemble of 1.34m×0.6m×1.5m elements, and the pier was modeled by the assemble of 0.25m×0.4m×0.2m elements.

In the analytical model, the ground was moeled by the fixed rigid element, and the footing was placed on the ground. The strength between the ground and the footing is the same as the strength of concrete, but no failure occured.

The interval of the springs and dashpots is the 1/4 of the shortest edge based on the finding from the previous study [5]. The total number of elements is 2828, the time interval used is 1.0×10^{-5} second.

3.3 Natural frequency of analytical model

The constant acceleration of 100gal with the duration of 0.2 second was input to the model to cause the free vibration assuming that the no failure occurs. The accelerations at the top of the pier were computed for both the longitudinal and transverse directions, and the dominant frequency was obtained by the Fourier transformation. The 1st natural frequencies were found to be 10.0Hz and 20.3Hz, respectively, for the longitudinal and transverse directions.

3.4 Input ground motion

The acceleration record observed at the Kawaguchi Branchi, Nagaoka City Hall during the 2004 Niigata-ken Chuetsu Earthquake was input to the model. The location of the observation point and the bridge is shown in Fig. 5. The acceleration with the duration of 13 second which has large

Fig.5 – Observation point and Uonogawa bridge

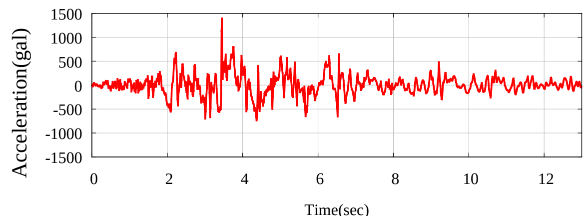

(a) *x* (longitudinal) component

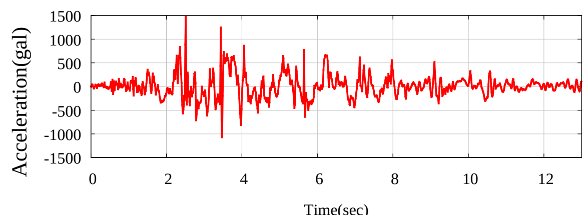

(b) *y* (transverse) component

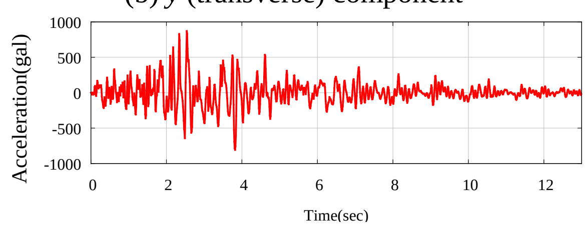

(c) *z* (vertical) component
Fig.6 – Input acceleration

(the 2004 Niigata-ken Chuetsu Earthquake)

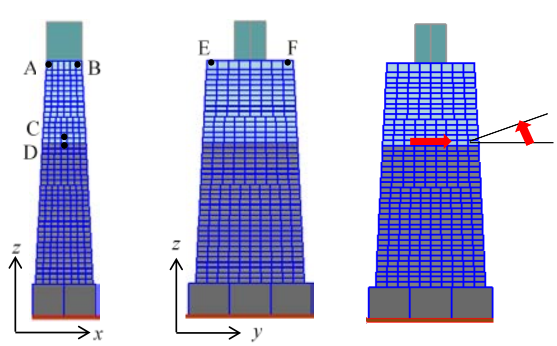

Fig.7–The location where the displacement responses are computed

amplitude was extracted. The acceleration in the NS and EW components were transformed into the longitudinal and transverse components, and 3 components in the longitudinal, transverse and upward directions shown in Fig.6 were input.

3.5 horizontal dislocation at the cold joint and the rotation angle of the pier above the joint

To obtain the horizontal dislocation at the cold joint and the rotational angle of the pier above the joint, the displacement response at 6 points shown in Fig.7 was computed. By taking the difference of relative displacement at point C and D, the horizontal displacement in x and y directions are obtained. The rotational angle to the x axis is obtained by dividing the difference of displacement response between A and B points by their horizontal distance. In the same manner, the rotational angle to the y axis is obtained by dividing the difference of displacement response between E and F points by their horizontal distance.

3.6 Results

3.6.1 Seismic behavior

Seismic behavior is shown in Fig.8. The left figure is the whole view, and the right one is the enlarged view around the cold joint where the danage is concentrated. In the enlarged view, the blue color indicates the outline of the element, the light blue indicates the tensile failure, the green indicates the shear failure, and the red indicates the compression failure. It is found that the most of the failure was caused by the tensile failure.

Since the tensile strength of cold joint is assumed to be 0 N/m^2, the tensile failure occurred immediately at the cold joint, and then the tensile failure occurred in the lower concrete pier in the south-west and south-east side at 2.23 and 2.52 second, respectively. The tensile failure then occured around all corners of the lower concrete pier, especially in the south-east side.

Fig.8 (e) indicates the damaged situation after the earthquake. The lower concrete pier below the cold joint was heavily damaged, but the upper concrete pier had less damage. The reason will be explained later.

The time history of horizontal dislocation in the transverse direction and the rotation angle at the top of the pier around the longitudinal direction is shown in Fig.9. The residual horizontal dislocation by the analysis is about 9 cm, which was smaller compared to the actual dislocation of 40 cm. The paramters used in the anaysis was based on the experimental results of the plain concrete piear in Wakayama Prefecture, and there

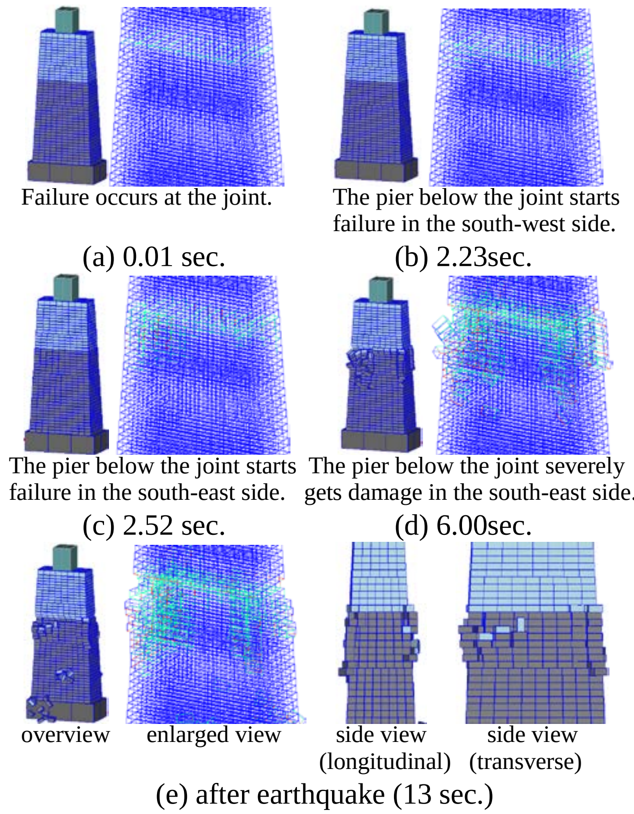

Fig.8 – Seismic behavior

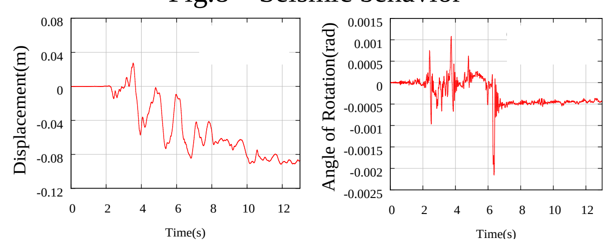

Fig.9 – Horizontal dislocation in *y* (transverse) direction (left) and rotational angle at the top of the pier around *x* (longitudinal) direction (right)

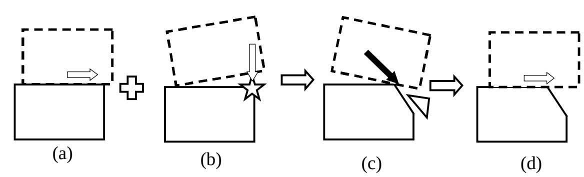

Fig.10 – Damage occurrence mechanism

(a) Friction force occurs to the lower part in the horizontal direction due to the sliding of the upper part.
(b) Collision force occures to the lower part in the vertical direction due to the rocking of the upper part.
(c) Sum of the friction force and the collosion force work in the diagonal direction, and the lower part experiences the tensile failue in the corner.
(d) Due to the failure of the corner, the friction force reduces, and the upper part becomes more easy to slide.

is a possibility that the analytical joint strength was stronger compared to the actual strength of pier 14 of Uonogawa bridge. It was also found that the small residual rotational angle remained due to the failure of the lower concrete.

Although the horizontal dislocation at the cold joint was underestimated, the damage pattern was successfully traced that the damage occurs to the lower pier below the cold joint.

3.6.2 Damage occurrence mechanism

Next, damage occurrence mechanism is investigated by comparing the time history of horizontal dislocation and rotation angle (Fig.9) with the seismic behavior (Fig.8).

Horizontal dislocation shows negative value around 2.2 second which means that the upper part slides in the negative direction of *y* axis with regard to the lower part. At this situation, the friction force acts at the top of the lower part in the negative *y* direction. The collosion force also acts to the lower part due to the rocking of the upper part. The rocking is confirmed from the fact that the rotation angle takes large value at 2.2 second. This horizontal friction force (negative *y* direction) and vertical collisiong force (negative *z* direction) becomes the obliquely downward force and this causes the tensile failure at the corner of the lower pier.

Fig.10 illustrates this failure occurence mechanism. The resultant force of friction and collosion generates the tensile stress to the corner of the lower part and the compression stress to the corner of the upper part, which is the reason why the severe damage only occurs to the lower part.

4. Investigation of effectiveness of seismic measures

4.1 Seismic measures

The most general seismic measures for the bridge pier is the RC jacketing method [9]. However, if the bridge pier is located inside the river, the seismic measures which does not increase the section area of bridge pier is preferred. Therefore, this study deals with two seismic measures which do not increase the section area proposed by West Japan Railway Company, namely H-shaped steel bar method and steel plate lining method. The same input ground motion with section 3 is used.

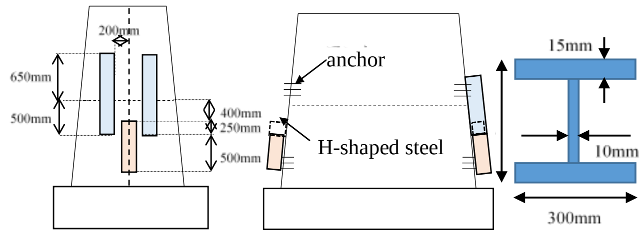

(a)side view (longitudinal direction) (b)side view (transverse direction) (c)section of H-shaped steel

Fig.11–H-shaped steel bar method

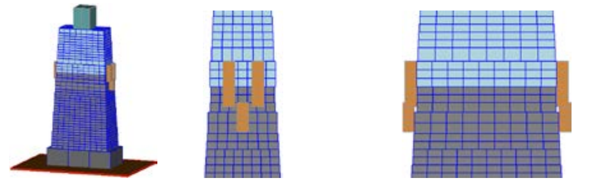

overview side view (longitudinal direction) side view (transverse direction)

Fig.12–Analytical model with H-shaped steel bar

Table 2 Material properties of steel

(a) Material Properties

Density(kg/m^3)	7.85×10^3
Young's modulue(N/m^2)	2.0×10^{11}
Poisson's ratio	0.30

(b)Strength between elements

	H-shaped steel	Steel plate	between steel and concrete
Tensile strength (N/m^2)	3.1×10^8	2.33×10^8	3.29×10^8
Cohesion (N/m^2)	1.79×10^8	1.35×10^8	1.897×10^8
Friction angle (rad)	0	0	0
Compression strength (N/m^2)	3.1×10^8	2.33×10^8	3.29×10^8

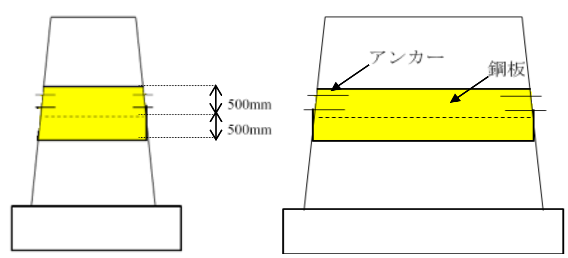

(a)side view (longitudinal direction) (b)side view (transverse direction)

Fig.13–Steel plate lining method

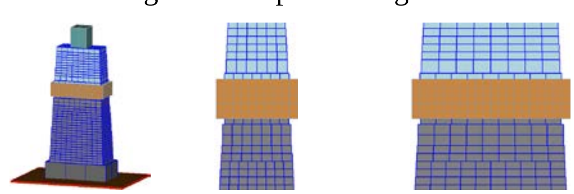

overview side view (longitudinal direction) side view (transverse direction)

Fig.14–Analytical model with steel plate lining

4.1.1 H-shaped steel bar method (Figs.11, 12)

This method uses six H-shaped steel bars to resist against the horizontal dislocation. Four bars are set at the upper part (two at each side) to resist the horizontal dislocation in the transverse direction. Two bars are set at the lower part (one at each side) between aforementioned 4 bars attached to the upper part to resist the horizontal dislocation in the longitudinal direction. If the cold joint is fully fixed, then the pier bottom gets damaged. Therefore, this method permits the rocking of the upper part to prevent the damage at the pier bottom. H-shaped steel made by SM490 was fixed to the concrete pier by the anchor of SD345 with the radius of 19mm and the length of 427mm. The table 2 indicates the material properties and strength regarding H-shaped steel. The values are determined following the specification for railway structures [10]. The anchor is not directly modeled, and the effect of anchor is included in the strength between H-shaped steel bar and concrete. It is assumed that the anchor has large strength enough not to get damaged.

The analytical model of the pier with H-shaped steel bar method is shown in Fig. 12. The number of elements is 2717. For simplicity, the section of H-shaped steel bar is modeled with square with the length of 300mm. The density is adjusted to have the same weight and the Young's modulus is also adjusted to have the same bending stiffness.

4.1.2 Steel plate lining method (Figs.13, 14)

The steel plate with the width of 2mm covers the pier to prevent the horizontal dislocation at the cold joint as shown in Fig.16. The plate is fixed to the upper pier by the anchor. The plate is not attached to the lower pier and the rocking is permitted. The strength of steel plate is shown in Table 2. The material is made of SM400 and the values are determined based on the specifications for railway structures [10]. The strength between the steel plate and the upper pier shown in Table 2 is strong enough to prevent the failure. The strength between the steel plate and the lower pier is assumed to be 0.

The analytical model is shown in Fig.14. The total number of elements is 2967. The assumed steel plate has the thickness of 12mm, but the plate was modeled with the cube with 200mm length since the smaller time interval is required for the smaller elements. The Young's modulus is adjusted to have the same bending stiffness.

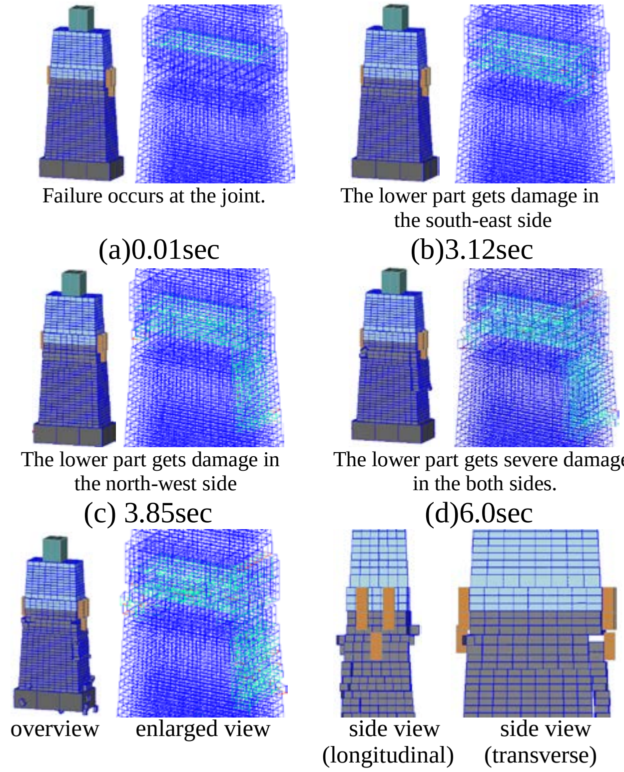

Fig.15 – Seismic behavior (H-shaped steel bar method)

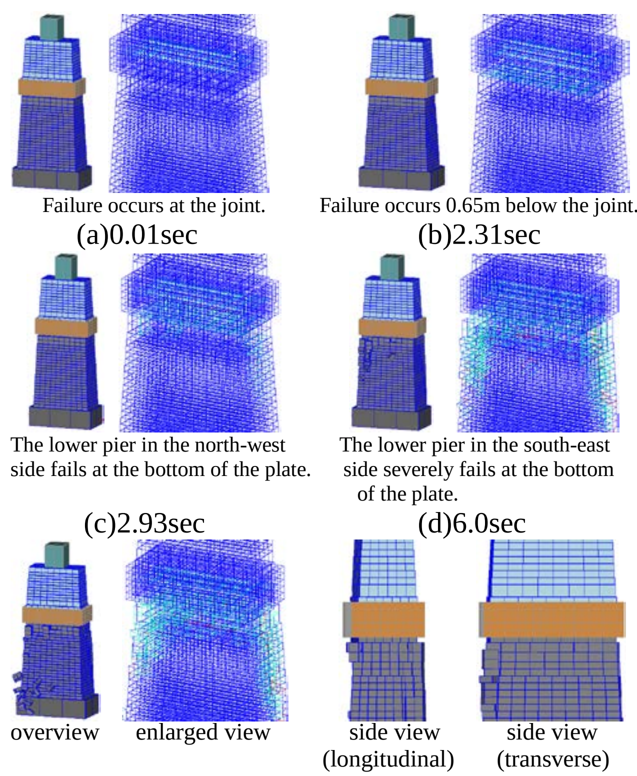

Fig.16 – Seismic behavior (Steel plate lining method)

4.2 Seismic behavior with seismic measures

The seismic behavior with two seismic measures are shown in Figs.15 and 16, respectively. The time history of horizontal dislocation at the joint and the rotational angle at the top of the pier is shown in Figs. 17 and 18.

4.2.1 H-shaped steel bar method (Fig.15)

The failure occurred immediately at the cold joint as shown in Fig.15(a). Then the H-shaped steel bars collided with the lower pier, and the tensile failure occurred at 0.65m lower from the cold joint at 3.12 sec. Then the crack propagated due to the repated collision, and the H-shaped steel bar attached to the lower pier collapsed due to the failure of concrete, and the restriction against the horizontal dislocation in the longitudinal direction is lost since there are no interlocking anymore between the H-shaped steel bars attached to the upper and lower piers.

4.2.2 Steel plate lining method (Fig.16)

The failure occurred immediately at the cold joint as shown in Fig. 16(a). Since the bottom of the steel plate collided with the lower pier, the tensile failure occurred at the collision point at 2.31 sec as shown in Fig.16(b). The upper pier showed rocking behavior, and the steel plate repeatedly collided the lower pier, and the failure proceeded (Fig.16(c)). Finally, the concrete piece fell at the south-east and north-west sides of the lower concrete (Fig.16(d)). Since the steel covers the pier, failure occurred at all sides (Fig.16(e)).

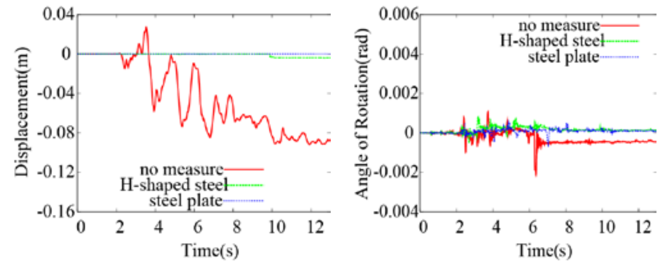

Fig.17 – Comparison of horizontal dislocation in *y* (transverse) direction (left) and rotational angle at the top of the pier around *x* (longitudinal) direction (right) among no measure, H-shaped steel bar method, and steel plate lining method

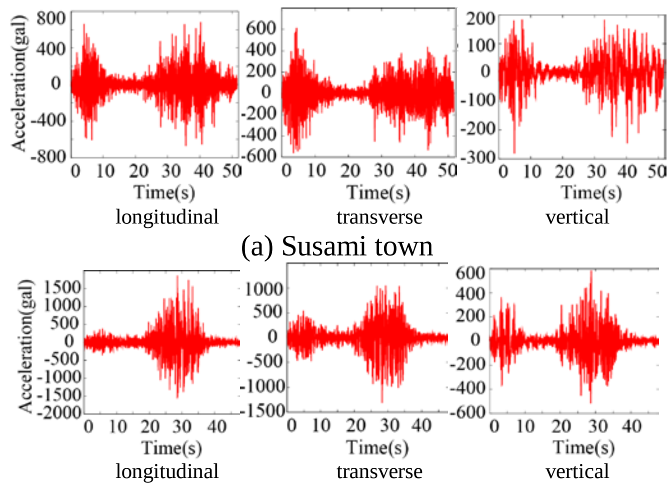

Fig.18–Input ground motion of Nankai trough earthquake

4.2.3 Comparison of horizontal dislocation and rotational angle (Fig.17)

The horizontal dislocation is reduced to almost 0 due to the both seismic measures. The maximum and residual values of the rotational angle at the top of the pier is also reduced due to the both seismic measures. However, there is a possibility that the larger horizontal dislocation will occur if the input ground motion with larger duration is input.

5. Evaluation of seismic safety during Nankai trough earthquake

5.1 Input ground motion

It is assumed that pier 14 of Uonogawa bridge is located in Wakayama Prefecture, and suffer from the shaking of Nankai trough earthquake. Two input ground motions are input as shown in Fig.18, one is an estimated wave in Susami Town, and the other is an estimated wave in Inami Town near Kisei main line of West Japan Railway Company. The engineering bedrock ground motion of “landward case” for Nankai trough earthquake provided by Central Disaster Prevention Council was transformed to the surface ground motion by the multiple reflection theory using the boring data.

5.2 Results

Figs.19, 20 and 21 indicate the damaged situation after the earthquake for the cases without measure, with the H-shaped steel bars and with the steel plate. Fig.22 indicates the time history of horizontal dislocation in *y* (transverse) direction and rotational angle at the top of the pier around *x* (longitudinal) direction among three cases.

5.2.1 Susami town

As for the case without measure, even though the duration of ground motion is longer, the damaged area is narrower than that by the Niigata-ken Chuetsu Earthquake since the acceleration is smaller. The maximum horizontal dislocation is 4.5cm in the transverse direction, and the lower pier than the cold joint got failed. The damage occurrence mechanism was same with that by the Niigata-ken Chuetsu Earthquake.

As for the case with seismic measures, the horizontal dislocation became almost 0, and the damage around the joint reduced for both measures. However, the slight damage can be seen at the pier bottom for the case with steel plate. The reason is considered that the horizontal inertia force of upper pier was transformed to the pier bottom due to the steel plate.

5.2.2 Inami town

As for the case without measure, since the ground motion of Inami town has larger amplitude, the severer damage occurred to the lower pier than that by the Niigata-ken Chuetsu Earthquake and that by the ground motion in Susami town. Even though the damage was severest, the horizontal dislocation at the cold joint was 5cm which was almost the same with that of Susami Town.

As for the case with the H-shaped steel bars, all H-shaped steel bars collapsed from the pier, and the horizontal dislocation at the cold joint could not be prevented. This seismic measure was found to be ineffective for the ground motion with larger amplitude and longer duration.

As for the case with the steel plate, the horizontal dislocation at the cold joint was almost reduced to 0. However, the severe damage occurred to the lower pier due to the collision between the steel plate the lower pier.

In summary, the steel plate lining method was more effective in reducing the horizontal dislocation at the cold joint for both ground motions, but the structural damage could not be prevented, and the severer damage is expected for the ground motion of Inami town.

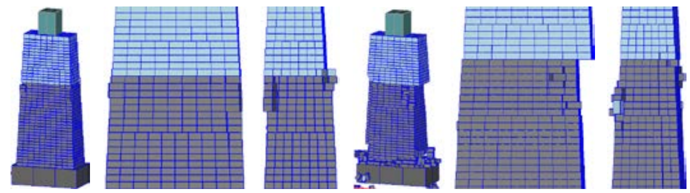

overview side view (longitudinal) side view (transverse) overview side view (longitudinal) side view (transverse)

(a) Susami town (b)Inami town

Fig.19–Seismic behavior (no measure)

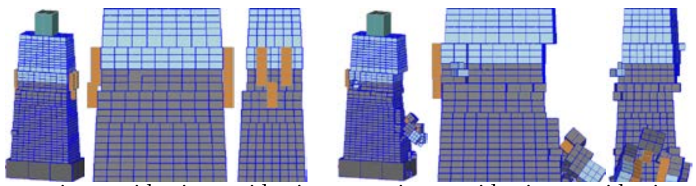

overview side view (longitudinal) side view (transverse) overview side view (longitudinal) side view (transverse)

(a) Susami town (b)Inami town

Fig.20–Seismic behavior (H-shaped steel bar method)

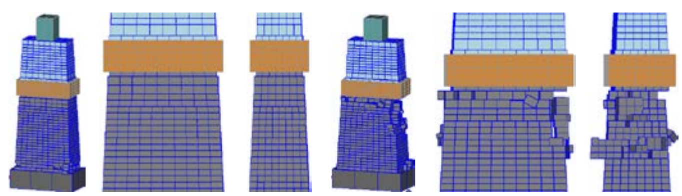

overview side view (longitudinal) side view (transverse) overview side view (longitudinal) side view (transverse)

(a) Susami town (b)Inami town

Fig.21–Seismic behavior (Steel plate lining method)

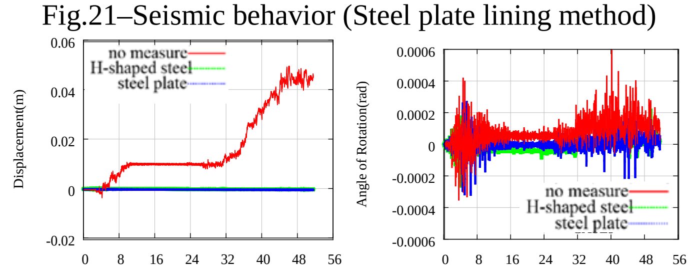

(a) Susami town

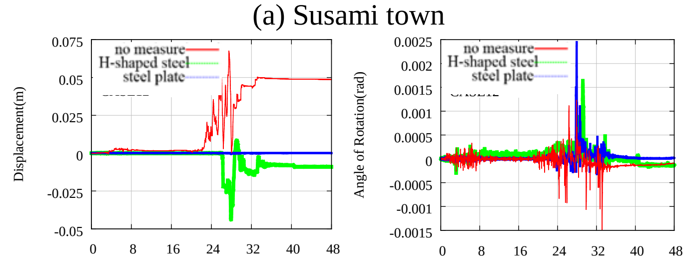

(b) Inami town

Fig.22 – Comparison of horizontal dislocation in *y* (transverse) direction (left) and rotational angle at the top of the pier around *x* (longitudinal) direction (right) among no measure, H-shaped steel bar method, and steel plate lining method

6. Conclusion

The seismic behavior of pier 14 of Uonogawa bridge was analyzed using the refined DEM, and the damage occurrence mechanism was investigated. The damage to the lower pier under the cold joint was occurred as tensile failure caused by the combination of the horizontal friction force and the vertical collision force. Next, the effectiveness of two seismic measures, the H-shaped steel bar method and the steel plate lining method were investigated. Even though the horizontal dislocation could be reduced, but the damage could not be prevented since the H-shaped steel bar and steel plate collides with the lower concrete pier. Lastly, two estimated ground motion of the Nankai trough earthquake were input to the structure with no measure and the structure with the seismic measures. For the model with no measure, the damage occurrence mechanism was same between Niigata-ken Chuetsu and Nankai trough earthquakes, but the severer damage was found for the ground motion in Inami town. The steel plate lining method was found to be more effective in reducing the horizontal dislocation at the cold joint, but could not prevent the structural damage of the lower pier.

7. Acknowledgement

This research was supported by West Japan Railway Company.

8. References

[1] Hakuno, M, Fujino Y, Katada T, Matsubara K (1979): Report of damage survey of 1978 Off Miyagi Prefecture earthquake, *Bulletin of the Earthquake Research Institute*, University of Tokyo, **54**, 351-398.

[2] Morikawa H, Fukushima Y (2004): Damage to civil engineering structures during 2004 Niigata-ken Chuetsu earthquake, *Research Reports on Earthquake Engineering*, Center for Urban Earthquake Engineering (CUEE), Tokyo Institute of Technology, **92**, 43-56.

[3] Disaster Investigation Team of Kyushu Institute of Technology (2000): Preliminary report of second damage survey of 2004 Niigata-ken Chuetsu earthquake, http://www.civil.kyutech.ac.jp/pub/kosa/ijikenHP/tyuuetujisin20041025.pdf [Last accessed: Sept 4, 2015].

[4] Second survey team of Kanto branch of JSCE (2004): Damage survey of Niigata-ken Chuetsu earthquake, Survey report of second survey team of Kanto Branch of JSCE, http://www.fps.chuo-u.ac.jp/~hrsk/earth/2004-niigata/files /nogami.pdf [Last accessed: Sept 4, 2015].

[5] Furukawa A, Kiyono J, Toki K (2011): Proposal of a Numerical Simulation Method for Elastic, Failure and Collapse Behaviors of Structures and its Application to Seismic Response Analysis of Masonry Walls, *Journal of Disaster Research*, **6**(1).

[6] Lourenco P.B (1994): Analysis of masonry structures with interface elements, theory and applications, *TU-DELFT report*, Delft University of Technology, Faculty of Civil Eng., 03-21-22-0-01.

[7] Sakaoka K, Doi T (2015): Fundamental investigation on characteristics of cold joint of plain concrete pier, *Proceedings of 70th annual conference of Japan society of civil engineers*, V-114.

[8] Railway Technical Research Institute (2004): *Design Standards for Railway Structures and Commentary* (*Concrete structures*), Maruzen.

[9] Sugisaki H, Kobayashi K (2007): Reversal cyclic loading test of plain concrete piers with construction joint retrofitted by RC jacketing method, *Proceedings of the Japan Concrete Institute*, **29**(3), 1093-1098.

[10] Railway Technical Research Institute (2009): *Design Standards for Railway Structures and Commentary* (*Steel and Composite Structures*), Maruzen.